20

Suspended Carbon Nanotubes: Applications in Physical Sensors and Actuators

Anupama B. Kaul and Larry Epp
Jet Propulsion Laboratory, California Institute of Technology, Pasadena, CA 91109 U.S.A.

1. Introduction

Carbon is truly an extraordinary material with physical structures spanning three-dimensional (3D) graphite, two-dimensional (2D) grapheme and zero-dimensional (0D) buckyballs or buckminster fullerine spheres. It is not surprising that the structural characteristics of carbon thus yield band diagrams displaying a diverse array of physical properties. When a 2D graphene sheet is rolled into a cylinder, a one-dimensional (1D) or quasi-1D form of carbon results, namely carbon nanotubes (CNTs), which have been one of the most extensively studied materials since their discovery (Ijima, 1991). A single rolled-up sheet of graphene results in a single-walled nanotube (SWNT) with a typical diameter of 1 – 2 nm. Multi-walled nanotubes (MWNTs) consist of concentric cylinders with an interlayer spacing of 0.3 – 0.4 nm, and diameters that are at least an order of magnitude larger than SWNTs, between 10 – 30 nm. The exceptional thermal, mechanical, electronic and optical properties of nanotubes (Dresselhaus, Dresselhaus, Avouris, 2001) has created a surge of applications, ranging from the use of CNTs as interconnects (Li *et al.*, 2003), heat transport materials (Yu *et al.*, 2006), novel transistors (Bachtold, *et al.* 2001), as well as optical materials (Homma *et al.*, 2009). The focus of this chapter is on the nanoelectronic applications of suspended carbon nanotubes, in particular their use as physical sensors and actuators.

Unlike 3D materials, when nanotubes are dispersed on a substrate, their properties are intimately influenced by the tube-to-substrate interactions, particularly those of SWNTs. For example, when diameter and helicity of SWNTs are controlled such that semiconducting tubes result (Odom *et al.*, 1998), no luminescence is detected for SWNTs lying on a substrate eventhough semiconducting SWNTs have a direct band gap (Lefebvre *et al.*, 2003). In addition, van der Waals interactions between CNTs and the substrate cause radial and axial deformations (Hertel *et al.*, 1998) which affect the electron transport properties of the tubes. The presence of the substrate beneath the tube can also influence heat dissipation mechanisms, which is an underlying motivation for using suspended CNTs as thermal conductivity based pressure sensors, and will be described in Section 2.2. Such sensors are important for vacuum-based microcavity applications (vacuum microelectronics, micro-eletromechanical-systems (MEMS) such as gyroscopes and RF MEMS switches). The high

modulus and low mass of the tubes also leads to resonators that operate at high frequency and exhibit a high quality factor (Q), which provides the basis for another physical sensing mechanism, namely mass sensing that will be described in Section 2.3. Other types of physical sensors, derived primarily from the integration of SWNTs in a MEMS platform, have also been fabricated and reviewed (Hierold *et al.*, 2007).

Suspended nanotubes can also be utilized as actuators, which serve as the active elements of many nano-electro-mechanical-systems (NEMS), and at length scales smaller than typical MEMS structures. The extremely high directional stiffness of CNTs (Salvetat *et al.*, 1999), their unique ability to accommodate very large mechanical strains (Yu *et al.*, 2000), coupled with their low mass and chemical inertness, collectively suggest that CNTs are ideal materials for NEMS. Nanotube based NEMS have already been demonstrated in applications ranging from nanotweezers (Kim & Lieber, 1999), memory devices (Rueckes *et al.*, 2000), and nanorelays (Dujardin *et al.*, 2005). In Section 3 and 4, the use of CNTS as NEMS actuators based on *laterally*, as well as *vertically* oriented tubes will be illustrated, respectively. These actuators can act as switches, potentially for low power, low leakage memory and logic applications, and due to their mechanical construct, such switches are also potentially more tolerant to radiation compared to solid-state transistors based on Si.

Throughout this chapter, we will present results from our own research conducted at the Jet Propulsion Laboratory (JPL), California Institute of Technology, where suspended or free-standing quasi-1D carbon nanostructures have been applied to both physical sensing (b. Kaul *et al.* 2009; d. Kaul 2009), as well as NEMS actuators (a. Kaul *et al.*, 2009; c. Kaul *et al.*, 2009; Kaul *et al.*, 2006).

2. Physical Sensor Applications

2.1 Methods of Suspension

The two primary approaches for forming suspended CNT structures are: a) post-growth release (Walters *et al.*, 1999), or b) where the tubes are grown across pre-fabricated trenches on a wafer using chemical vapor deposition (CVD) (Tombler *et al.*, 2000; Minot *et al.*, 2003). In both approaches, the AFM tip was used to mechanically strain the suspended tube(s) in order to understand how structural deformation affects the elastic strain in SWNT ropes (Walters *et al.*, 1999) and the electronic transport properties of individual SWNTs (Tombler *et al.*, 2000; Minot *et al.*, 2003). In our work at JPL, we have implemented both approaches to form suspended nanotube structures, but such structures have been exclusively used for device applications, specifically for physical sensing and NEMS actuators.

Post-growth release was utilized with critical point drying to form suspended SWNTs that were used for pressure sensing (b. Kaul *et al.*, 2009; d. Kaul, 2009). The operational mechanism of such sensors will be illustrated in Section 2.2. For the post-growth release approach, the SiO_2 beneath the SWNTs was etched in 10:1 Buffered-HF (BHF), which was followed by critical point drying. Simple drying techniques have been employed after HF etching to release < 1 μm long tubes by using the reduced surface tension of IPA (21.7 mN/m) (Nygard *et al.*, 2001), compared to that of DI water (72.8 mN/m), whereas the even lower surface tension of tetramethylsilane (10.2 mN/m) has also been utilized in other reports (Walters, 1999). For the long SWNTs used in our sensors (5 – 10 μm), which are more susceptible to surface tension stress upon wet-release, added precautions were taken that employed critical point drying. The electrical yield after release -- defined by the number of

electrically conducting devices -- was > 90%, but the resistance was always higher after release. The rise in resistance could be associated with the contacts where the tubes are likely to exhibit kinks that suppress conductance. It could also be due to HF damaging the SWNTs; clearly more work is necessary to fully characterize the extent to which HF damage is also involved.

We have also implemented the second technique to suspend tubes, where SWNTs have been grown across prefabricated trenches. Such structures were utilized for lateral NEMS actuators that will be discussed in Section 3.1. In earlier reports tubes were grown across prefabricated trenches, where the suspended tubes were over SiO_2/Si (Minot *et al.*, 2003) substrates. In contrast, we formed our suspended SWNTs over refractory Nb electrodes, which served as the pull-electrode to transiently charge the SWNTs in order to induce electromechanical switching. In general, the choice of the approach used to suspend tubes depends in part on the aspect ratio of the trenches, and on the quality of the tubes desired. For example, tubes that do not undergo post-growth processing are likely to be less defective, but such a technique is usually not feasible for forming suspended structures for low aspect ratio trenches below ~ 1:10; if the aspect ratio of the trench is too small, the tubes are likely to be undesirably draped on the substrate within the trench. This arises from the large amplitude vibrations that are thermally induced in the tubes from the high temperature CVD growth dynamics, increasing the likelihood of tubes attaching to the underlying substrate if the aspect ratio is too small.

2.2 Application in Pressure Sensors

Among the diverse variety of applications of CNTs, recently, CNTs have also been applied to pressure sensing based on the mechanism of piezoresistance (Grow *et al.*, 2005; Stampfer *et al.*, 2006). In these recently reported CNT pressure sensors (Stampfer *et al.*, 2006), metallic SWNTs were placed on membranes of atomic-layer-deposited (ALD) alumina, and a pressure differential across the membrane caused it to bulge, inducing strain in the overlying SWNT. Strain-induced conductivity changes were detected in non-vacuum environments (760-900 Torr).

Unlike the mechanism of piezoresistance, here we present a CNT pressure sensor that operates on the principle of thermal exchange between a voltage-biased CNT and the surrounding gas (b. Kaul *et al.*, 2009; d. Kaul, 2009). A recent article by Kawano (Kawano *et al.*, 2007) presents a sensing mechanism similar to that reported here, which utilized MWNTs grown using a localized synthesis process (Kawano *et al.*, 2006). Here we report on the device application of sensors based on SWNTs that were grown using conventional thermal CVD. Typical thermal conductivity gauges, such as Pirani or thermocouple gauges are physically large (volume ~ 10 cm^3) prohibiting their integration with many vacuum-encased Si-based micro-cavity applications (vacuum microelectronics, MEMS such as gyroscopes and RF MEMS switches). As a result of their large thermal mass, they are inherently slow, and also operate at high powers and temperatures.

With the advent of MEMS technology, miniaturized, low power pressure sensors were developed, representing the first application of bulk Si-micromachining (Peterson, 1982). Many of these Si-based transducers operate on the piezoresistive or capacitive principle (Esashi *et al.*, 1998) and obtaining wide-dynamic range has been challenging, which is especially important in micro-cavity applications. Due to the small volumes in micro-

cavities, outgassing can cause large pressure changes over short times, affecting device performance.

We present a miniature SWNT-based thermal conductivity gauge (volume ~ 10^{-4} cm^3) that operates at low power (nW-μW) and low temperature, and exhibits a wide dynamic range (760 Torr-10^{-6} Torr). Due to the reduced dimensionality for thermal conduction and phonon relaxation in 1D materials, transport is strongly influenced by environmental factors. The high surface area of the 1-D SWNT, along with the high temperature coefficient of resistivity (TCR) of diffusively contacted 5-10 μm long tubes, greater pressure sensitivity is enabled compared to thin-film or bulk conductors. Moreover, when the CNT is suspended, heat dissipation via the substrate is minimized, increasing sensitivity at even lower pressures. We have carried out an investigation of such devices for their feasibility as vacuum gauges.

A schematic of the device is shown in Fig. 1a where the starting substrate was a thermally oxidized Si <100> wafer. Patterned CVD growth of SWNTs using Fe-catalyst was performed, which was followed by e-beam deposition of Au/Cr electrodes (250 nm/5 nm) patterned by liftoff. In order to release the devices, the SiO_2 beneath the SWNTs was etched in BOE which was followed by critical point drying described in Section 2.1. A low magnification SEM image of a completed device is shown in Fig. 1b, which also shows the wire-bonds for electrically contacting the devices. The high magnification SEM image in Fig. 1c indicates a tube traversing the electrode, where typical tube lengths were 5 – 10 μm.

(a)

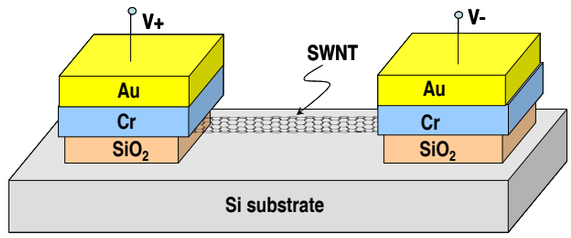

(b)

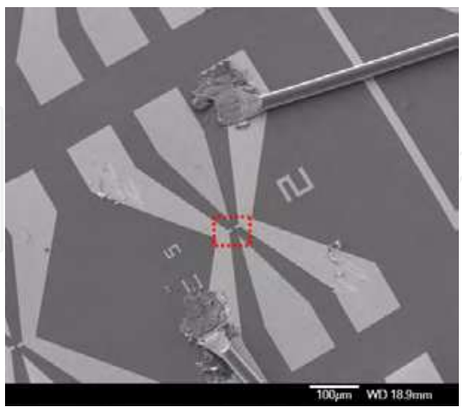

(c)

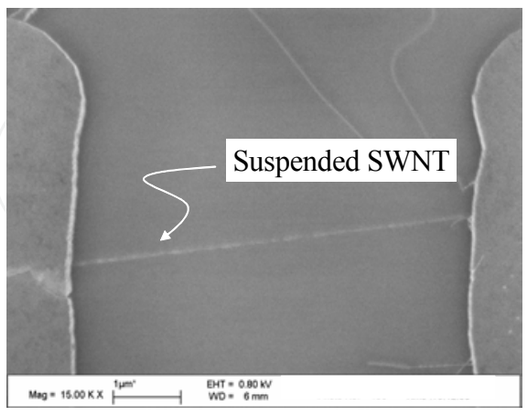

Fig. 1. a) A schematic of the CNT pressure sensor where the SWNT is suspended. b) Low magnification SEM image of wire-bonded CNT vacuum gauge. Area highlighted by dashed lines indicates the region observed in the high magnification image in (c), where the typical SWNT lengths were 5-10 μm. Trench depth was ~ 310 nm (b. Kaul *et al.*, 2009).

Though the number of tubes that nucleate from the catalyst site can be controlled, to some extent, by the size of the catalyst island in thermal CVD, multiple tubes are shown in the SEM image of Fig. 1c. However, the growth of some of the tubes is seen to terminate prior to the mid-gap region (bottom of right electrode), while other tubes are oriented in a growth direction that does not allow them to bridge the gap to the opposite electrode (top of right electrode). The image in Fig. 1c thus, shows a single tube traversing the gap between the left and right electrodes. However, it is likely the presence of multiple tubes bridging the gap may enhance sensor robustness, and hence performance for practical applications. In conjunction with measuring the pressure response of unreleased and released CNT devices, a thin film meander resistor was also fabricated and pressure response measured for comparative purposes.

The current that passes through a voltage biased wire lying on a substrate induces joule heating. This heat can dissipate via several mechanisms, including the substrate (E_s), radiation (E_r) or the gas (E_g) (Alvesteffer *et al.*, 1999) as shown by Eqn. (1) below; the input power supplied to the bias element is represented by an energy E_t where,

$$E_t = E_s + E_r + E_g \tag{1}$$

The heat dissipated through the substrate is

$$E_s = (K\Delta TA)/L \tag{2}$$

where A is the area through which heat transfer occurs, K is the thermal conductivity of the SiO_2, ΔT is the temperature difference between the current carrying element and the substrate and L is the distance from the element to the substrate. Radiative losses are given by (3) where σ is the Stefan-Boltzmann radiation constant, ε is the thermal emissivity of the element, and T_h and T_a are the temperatures of the element and ambient, respectively.

$$E_r = \sigma\varepsilon(T_h^4 - T_a^4)A \tag{3}$$

Finally, heat dissipation by the gas is given by E_g,

$$E_g = \alpha_r \Lambda_t AP(T_h - T_a)\sqrt{\frac{273}{T_h}} \tag{4}$$

where α_r is the accommodation coefficient, Λ_t is the free molecule thermal conductivity, A is the surface area of the element, and P is the pressure. While the radiative and substrate losses become more significant at low pressures, the thermal conductivity of the gas is a predominant loss mechanism in the viscous flow regime ($0.01 < K_n < 10$, where K_n is Knudsen's number). The heat dissipation in this regime depends linearly on pressure as illustrated by Knudsen's formula (Eqn. 4).

Shown in Fig. 2a, is the normalized current as a function of pressure for the thin-film meander resistor and a CNT device, both of which are biased at a few watts of power. The thin film resistor initially shows a conductance increase (up to about 200 Torr), a plateau region of constant current, and then current decreasing below about 20 Torr; the percent

change in current is < 1%. In contrast, the CNT device, shows a rapid and continuous decrease in current from ambient to ~ 40 mTorr, with more than 35 % change in conductance.

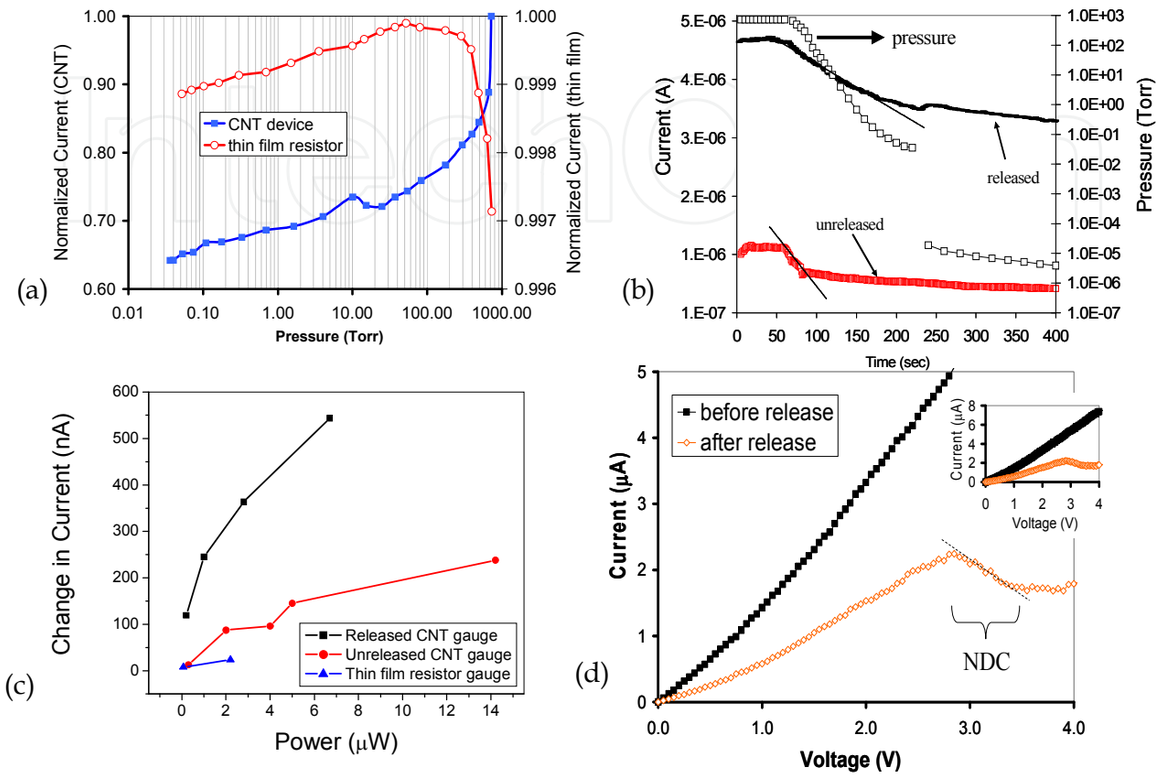

Fig. 2. a) Normalized current-pressure response at 2 μW for thin film resistor and unreleased CNT device. The conductance change is smallest for thin film resistor (< 1 %) while the conductance continues to decrease for the CNT device by about 35% at 35 mTorr. b) Absolute current variation for released and unreleased device vs. time/pressure at ~2 μW. The released device shows a higher rate of conductance change down to ~10^{-6} Torr possibly due to minimizing heat loss through the substrate. c) Net current change from ~ 5 x 10^{-6} Torr to ~ 8 x 10^{-7} Torr for released and unreleased CNT sensors as a function of bias power. The thin film resistor gauge was the least sensitive. The largest change in conductance is for released device at high power levels. d) The conductance of an unreleased SWNT device increases monotonically as the bias is increased, but after substrate removal, current saturation and a negative differential conductance (NDC) regime is observed in this device at high biases, which is attributed to the high optical phonon density in suspended tubes. Inset shows a higher current scale (b. Kaul *et al.*, 2009; d. Kaul, 2009).

At low pressures (< 100 mTorr), conduction through the gas becomes less significant and other pressure independent mechanisms such as radiative losses and solid-state conduction through the substrate tend to dominate, as seen by Eqns. 2 and 3. Radiative losses are significant only when temperatures exceed > 200 ºC, and although radiative losses may be minimal at the low operational temperatures (or power) of our devices, the losses through the substrate have been calculated to be significant in the low vacuum regime. We

implemented post-growth release to remove the oxide beneath the tubes as described, in order to suspend the tubes and measured their pressure response.

Shown in Fig. 2b is the pressure response of a device before and after the CNT was released from the SiO_2 substrate. As it can be seen, the released CNT device has a continued decrease in conductance well into the 10^{-5} Torr range while the unreleased device shows little variation after about ~ 100 sec (~ 1 Torr), in this case. This data appears to confirm that by removing the substrate underneath the current carrying element, sensitivity is increased to the lower pressure ranges.

The increase in sensitivity after substrate removal is perhaps better exemplified by the data in Fig. 2c which shows the net current change (ΔI) for released and unreleased device in the pressure range of ~ 5 x 10^{-6} Torr to ~ 8 x 10^{-7} Torr. In both cases, ΔI increases with power but the released device has a three times larger change than that of the unreleased device (at a power of ~ 6 μW, $\Delta I_{released}$ ~ 550 nA, compared to $\Delta I_{unreleased}$ ~ 150 nA). The relationship of power effecting sensitivity appears to be in agreement with Fig. 2c, and the combined results suggest that the greatest sensitivity is expected for the released devices operated at high power.

While the increased current sensitivity with substrate removal can be explained on the basis of heat minimization through the substrate, the reduced dimensionality for phonon scattering in 1-D systems, in particular suspended SWNTs, can cause unique effects to arise at large bias voltages and power. At high fields, a large nonequilibrium optical phonon population exists in suspended SWNTs and their long relaxation times result in non-isothermal conditions along the length of the tube. The I-V characteristic of both suspended and unsuspended SWNTs has been iteratively calculated (Pop *et al.*, 2005), by modeling the occupation probability of both optical and acoustic phonons at high biases, according to $I = \frac{V}{R(V,T)}$ where,

$$R(V,T) = R_c + \frac{h}{4e^2}\frac{\left\lfloor L + \lambda_{eff}(V,T)\right\rfloor}{\lambda_{eff}(V,T)} \tag{5}$$

Here, R_c is the contact resistance, L is the length of the nanotube and λ_{eff} is the sum of the acoustic, optical (emission) and optical (absorption) mean free paths derived from the Bose-Einstein phonon distribution. This analysis showed that in unsuspended tubes the I-V characteristic increases monotonically at high voltages suggestive of isothermal conditions, since the substrate facilitates in the relaxation of optical phonons emitted through electron scattering. In contrast, the current in the suspended tube saturates and a negative differential conductance (NDC) regime is encountered, which cannot be explained by velocity saturation (at ~ 5 kV/cm).

We have observed NDC in our suspended SWNT devices as shown by the I-V characteristic in Fig. 2d, where such measurements were taken in air and at room temperature. The unreleased device shows a monotonic rise in conductance, while the current after release for the same device saturates at high bias, ~ 2.8 V in this case, and enters a NDC regime. A peak conductance I_{peak}, where

$$I_{peak}(\mu A) = \frac{10}{L(\mu m)} \tag{6}$$

has been calculated and depends inversely on the length of the tube (Pop *et al.*, 2005). In the device shown in Fig. 2d, the experimentally observed I_{peak} was ~ 2.1 μA which appears to be in rough agreement with the expected value since the electrode spacing (and hence tube length) for this device was ~ 6 μm. Measurements show pressure sensitivity increases as the bias voltage or power are increased, but the released devices showed a more pronounced effect with power, as shown in Fig. 2c. The large optical phonon density in suspended SWNTs at high fields, with their long lifetimes may play an important role in determining the rate of temperature rise in the tubes, which can be exploited for their utility as thermal conductivity-based pressure or gas sensors.

2.3 Application in Mass Detection

While the pressure sensing mechanism described in 2.2 relied on suspended tubes that are stationary, the tubes in such bridge-type structures can also be driven into vibration or resonance by an external pertubation, forming the basis for yet another type of sensing mechanism, namely mass sensing. Much like a guitar string, the vibration frequency of the tube or suspended beam is a sensitive function of its total mass. The smaller the total mass, the more sensitive it will be to the external peturbation, and the higher is its resonance frequency. The addition of any adsorbed mass on the tube or beam will cause a shift in its resonance frequency, which can be measured and implemented for mass sensing.

Since sensitivity increases as beam dimensions shrink, there has been a constant push to drive the device dimensions to smaller and smaller length scales. For example, Si MEMS beams that resonate at RF frequencies, were used to detect species as small as bacteria and viruses as they adsorbed on a micromachined beam and caused a shift in its resonance frequency (Ilic *et al.*, 2004). More recently, lithographically fabricated NEMS beams with their even smaller masses, high frequency operation, and high Q's, were successfully used for the detection of protein molecules and nanoparticles (Naik *et al.*, 2009). Theoretical calculations suggest that mass sensitivity below a single dalton could be achieved by making NEMS beams even smaller; this approach may be used for weighing individual atoms and for performing mass spectrometry, for example in proteomics, using a large-scale array of such sensors.

Resonance phenomena has also been observed in SWNTs (Sazonova *et al.,* 2004; Peng *et al.*, 2006), which offer even more advantages than top-down fabricated MEMS and NEMS structures due to the remarkably high Young's modulus and light structure of SWNTs. Such suspended SWNTs have been shown to act as oscillators, where the resonance frequency was measured using an indirect mixing technique with a lock-in amplifier. More recently, resonance was also observed in metallic MWNTs by using a direct on-chip transmission measurement technique where an RF displacement current was detected as the tube was driven into resonance (Eriksson *et al.*, 2008). Suspended CNTs are attractive as mechanical resonators and have significant promise for mass sensing applications.

3. Actuators Based on Laterally Suspended Tubes

3.1 Actuators Based on Single Tubes

Besides physical sensing applications, suspended CNTs can also serve as actuators for NEMS. Such NEMS-based actuators can serve as switches exhibiting reduced leakage currents and power dissipation, when compared to Si transistors that are now facing

performance limitations as a result of continued miniaturization. Due to the capacitive nature of switching in solid-state transistors, such devices are also susceptible to radiation and extremes in temperature. Due to the "mechanical" construct of NEMS switches, they should be inherently more robust when operated in harsh environments. In this section, NEMS switches that are based on tubes oriented laterally or parallel to the substrate are discussed. For laterally-oriented tubes, switches based on single tubes are described, and then Section 3.2 follows with an overview of a technology where monolayer thick fabrics of tubes are used.

Electromechanical switching in CNTs was first observed by (Rueckes T. *et al*., 2000) where single-walled-nanotubes (SWNTs) were mechanically manipulated to form crossed structures with an air-gap. Switching has been demonstrated in deposited MWNT cantilever structures (Lee *et al*., 2004) that were fabricated using an AC electrophoresis technique. In addition, deposited MWNTs have also been used to demonstrate electrostatic switching, where individual tubes were located by SEM for subsequent e-beam and thin film processing (Cha *et al*., 2005). To date, switching in both SWNTs and MWNTs has been reported for the case of deposited tubes. Here the work on SWNT NEMS switches (Kaul *et al*., 2006) is presented, where the tubes are grown on-chip with patterned catalysts using materials that are compatible with the high temperature CVD synthesis of SWNTs.

As described in Section 2.1, besides post-growth release (Walters *et al*., 1999), nanotubes have also been grown across pre-fabricated trenches (Tombler *et al*., 2000; Minot *et al*., 2003) on a Si wafer. Unlike the latter structures where the tubes were suspended directly over SiO_2/Si substrates, in the application of laterally suspended SWNTs for NEMS applications presented here, suspended SWNTs were formed over a refractory metal electrode made from niobium (Nb). The Nb serves as the pull electrode to transiently charge the tube in order to induce electrostatic switching.

The process of formation is shown in Fig. 3a. In the first masking layer, active device regions in the PECVD SiO_2 were patterned to thin down the oxide from 200 nm to ~ 20 nm, which was comparable to the air gap of the switch. Nanotrenches that were as small as 130 nm were then defined using e-beam lithography. The nanotrenches were patterned using CF_4/O_2 RIE to etch the PECVD SiO_2 down to the Nb layer. For nanotube growth, catalyst was patterned by photolithography and liftoff of 0.5 nm Fe which was deposited by e-beam evaporation. The sample, with patterned Fe, was then placed in a CVD furnace for nanotube growth at 850 ^oC for 10 min using CH_4 and H_2 at flow rates of 1500 sccm and 50 sccm, respectively, where SWNT growth predominates. After CNT growth, the metal electrodes (Au/Ti) were patterned to contact the CNTs, using a bilayer AZ 5214/PMMA lift-off process, which results in easy lift-off of metal films due to an undercut in the PMMA layer. The top electrode metals Au/Ti were then deposited in an e-beam evaporator and lifted off in acetone. The high magnification SEM image of Fig. 3b depicts a nanotube crossing the trench.

The conductance between the left and right electrodes was measured and is shown in Fig. 4a, which yields a resistance of ~ 200 kΩ, much of which can be attributed to the high contact resistance between the CNT and Au/Ti electrodes. In general, these resistances typically ranged in value from tens of kΩ to tens of MΩ's, where the presence of multiple tubes can also contribute to the differences in resistance.

The actuation voltages were measured by applying a DC voltage between either the left or right electrode and the Nb pull electrode beneath the tube. As transient charge develops on

the tube with increasing bias voltage, the resulting electrostatic force is sufficient to overcome the elastostatic force and deflects the suspended tube down toward the pull electrode.

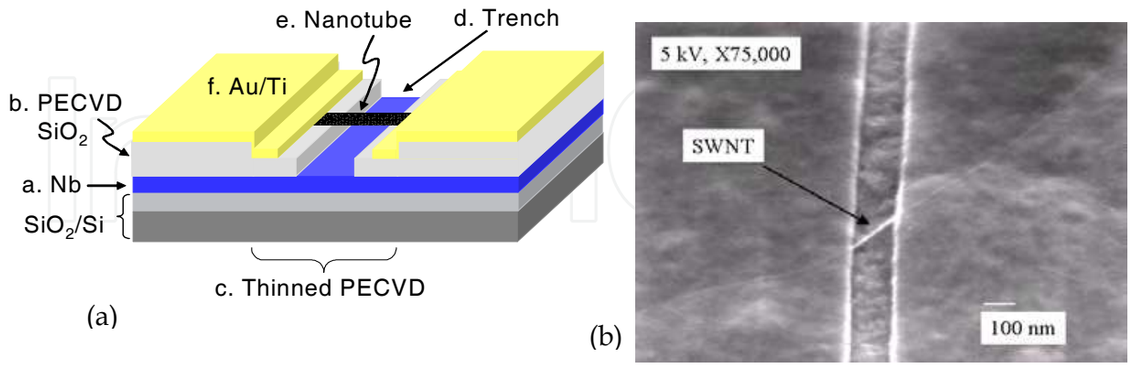

Fig. 3. a) Schematic shows a nanotube switch composed of (a) a 200 nm Nb film deposited using DC magnetron sputtering onto a thermally oxidized Si wafer followed by (b) a 200 nm PECVD SiO_2 layer. (c) Active device regions are etched in the PECVD SiO_2 layer to a thickness of ~ 20 nm, the height of the air gap for the switch. (d) Nanotrenches are defined using e-beam and etched to the Nb layer. (e) SWNT are grown from patterned Fe in a CVD furnace using CH_4/H_2 (1500 sccm/50 sccm) at 850 ^oC. (f) Electrodes are deposited using e-beam evaporated Au/Ti (220 nm/12 nm) which are patterned using a bilayer resist/PMMA process for easy lift-off. b) High magnification SEM micrograph showing a single nanotube bridging the 130 nm wide trench (Kaul *et al.*, 2006).

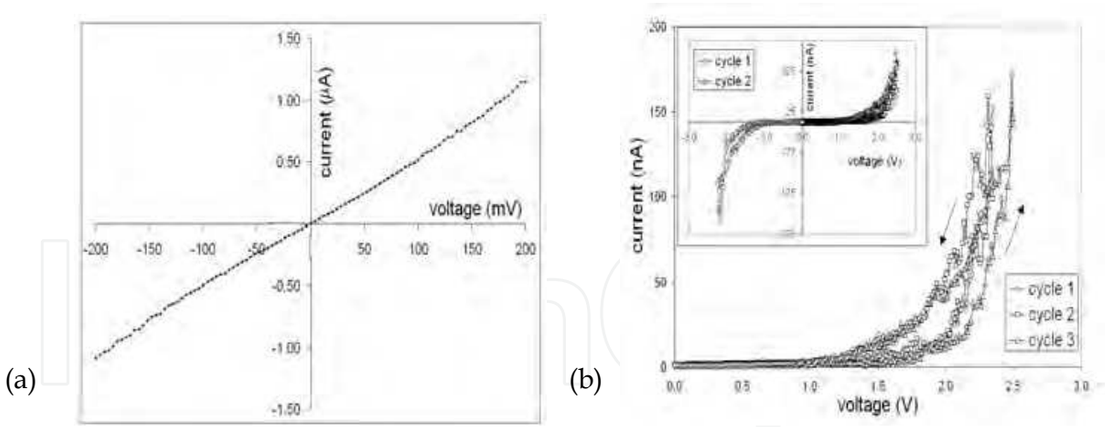

Fig. 4. a) Conduction measurements from the left Au/Ti electrode to the right electrode for a typical device gives R ~ 200 kΩ (trench width ~ 250 nm, 2 μm x 5 μm catalyst area). b) I-V characteristic of a device actuated over multiple cycles (250 nm trench width). The inset shows the ON state voltage to be similar in the forward-bias (pull electrode grounded) and reverse-bias (pull electrode positive) regimes, indicating that field emission is an unlikely possibility at these voltages (Kaul *et al.*, 2006).

Shown in Fig. 4b is an I-V characteristic of a device that was actuated over several cycles. Turn-on occurs at ~ 2.4 V in this case, with a slight variation with cycling that is also reported in other CNT (Lee, 2004) and MEMS switches. The rapidly rising current regime arises in both the forward-biased (pull electrode grounded) and reverse-biased (pull electrode positive) cases, as indicated by the inset of Fig. 4b, although the exact switching voltages are slightly different in the two cases, ~ 2.4 V (forward-biased) and ~ 2.2 V (reverse-biased). The differences in turn-on voltage can perhaps arise from the random distribution of metallic and semiconducting tubes observed in current SWNT growth processes, but still suggest that the differences in resistance between the ON and OFF states far outweigh any differences that may arise from contact resistances. As shown by the inset of Fig. 4b, this switching behavior is polarity independent, as would be expected for electrostatic actuation, and rules out field emission as a likely mechanism at these voltages. In general, the magnitude of the switching voltages in these air-bridge devices was a few volts and the switching times were determined to be a few nanoseconds.

3.2 Actuators Based on Fabrics of Tubes

While the previous section was focused on the electrostatic switching in NEMS devices comprising of individual SWNTs or MWNTs, monolayer thick fabrics of nanotubes are also being investigated and are a cornerstone of Nantero's mechanical memories (http://www.nantero.com/) that are currently under development. In this application, monolayer thick fabrics of CNTs are formed by dispersing a prepared solution of SWNTs in a solvent onto a substrate and evaporating the solvent. The resulting 1-2 nm thick film is then patterned using conventional lithography and monolithically integrated with other CMOS processes to form laterally suspended monolayer thick fabrics that can be switched electrostatically. Companies such as Nantero are developing this monolayer thick fabric fabric technology for making non-volatile memory elements for replacing Static-Random-Access-Memory (SRAM), Dynamic-Random-Access-Memory (DRAM) and Flash memory, for the defense, space, and commercial markets. Applications targeted are the formation of military and space-rated radiation-hard CMOS-CNT hybrid devices and circuits, and non-volatile memory products for the commercial marketplace.

4. Actuators Based on Vertical Tubes

4.1 Growth of Vertically Aligned Carbon Nanofibers

The discussion in Section 2 and 3 has been on the sensor and actuator application of tubes oriented parallel to the substrate. We now describe results from our research in forming tubes oriented perpendicular to the substrate, which are being developed for actuator applications for 3D electronics (a. Kaul *et al.*, 2009; c. Kaul *et al.*, 2009). The formation of vertically oriented tubes was enabled by implementing plasma-enhanced (PE) CVD, which enhances the alignment of the tubes, compared to CNTs synthesized using thermal CVD (c. Kaul *et al.*, 2009). Thermal CVD, which is a heavily utilized technique for the synthesis of CNTs, specifically MWNTs, results in 'bundles' of tubes largely perpendicular to the substrate. Inspection of MWNTs in such bundles reveals individual tubes growing in random directions and forming a 'matted' array. Often, this poor vertical tube alignment does not maximally utilize the exceptional 1D thermal, mechanical, electrical or optical

properties of the tubes, and reduces performance for certain applications, such as field emitters for flat panel displays or thermal interface materials for integrated circuits.
A technique which has emerged in recent years to ensure excellent vertical tube alignment is PECVD (Ren *et al.*, 1998), where the inherent E-field in the plasma allows tube growth in a direction parallel to the field. Shown in Fig. 5a is a DC glow discharge produced in our PECVD growth chamber at the JPL Microdevices Laboratory, where a uniform and stable discharge is seen over an area as large as 75 mm. Analysis of crystallinity of individual tubes synthesized using PECVD reveals graphitic structures where the graphene layers are inclined to the central axis; these structures are commonly referred to as carbon nanofibers (CNFs) and control over their physical orientation with the plasma is excellent. Various plasma sources have been employed for tube or CNF growth, such as microwave, inductively coupled plasma (ICP), DC and DC with hot filament (Melechko *et al.*, 2005).

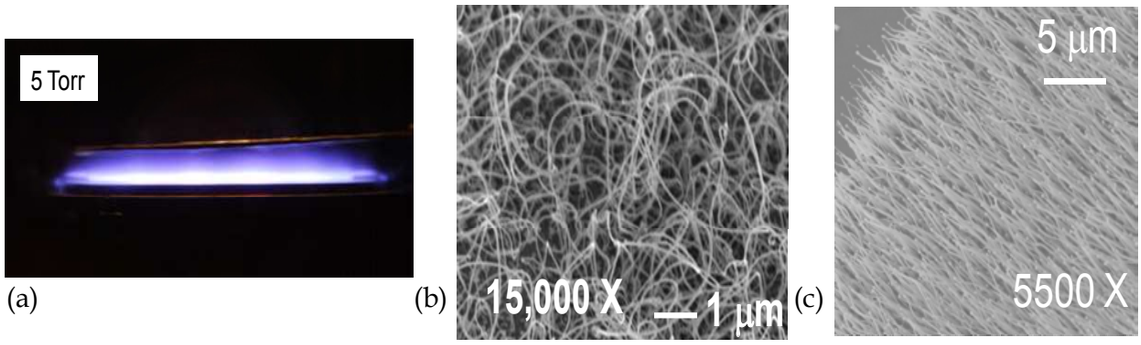

(a) (b) (c)

Fig. 5. a) The inset at the top showing a stable and uniform plasma over a diameter spanning ~ 75 mm. b) Unaligned tubes result when C_2H_2 and NH_3 are used in the absence of an E-field, where the substrate was degenerately doped Si with ~ 4 nm thick Ni catalyst. c) A high areal density of vertically aligned tubes was achieved using a 15 nm thick Ni film on degenerately doped Si, with 53 sccm of C_2H_2 and 90 sccm of NH_3 at 5 Torr and 300 mA (c. Kaul *et al.*, 2009). The image is taken where the SEM beam was at ~ 45° relative to the holder on which the sample was mounted.

When only C_2H_2 and NH_3 were present at a temperature of ~ 700 °C in the absence of an electric field, unaligned tubes resulted, as shown in Fig. 5b. In the presence of a stable plasma, a 15 nm thick Ni catalyst resulted in a large areal density of vertically aligned tubes, as shown in the SEM in Fig. 5c (sample holder is tilted at 45° with respect to the SEM beam). Although the growth temperature here was fixed to 700°C, prior work suggests there is a possibility for lowering this to temperatures more compatible with CMOS or low-temperature substrates (Hoffman *et al.*, 2003). In general, elevated temperatures cause the thin Ni catalyst film to dissociate into fine nanoclusters as a result of surface energy driving forces, where the clusters then serve as nucleation sites for tube growth. The plasma may also aid in catalyst particle fragmentation directly via ion bombardment, which may also contribute to heating the substrate surface indirectly.
The physical characteristics of the tubes were controlled to some extent with this bottom-up technique, by adjusting th growth parameters, such as growth pressure, catalyst thickness, and power during dc PECVD synthesis of the tubes. As an example, the SEM in Fig. 6 shows tubes of diameters ranging from 200 nm down to only 40 nm, which resulted from varying

growth parameters. Also, as is evident from this figure, a tip growth mechanism was operative, where the nominally pear-shaped nickel cap, remains on the tip as the tube grows.

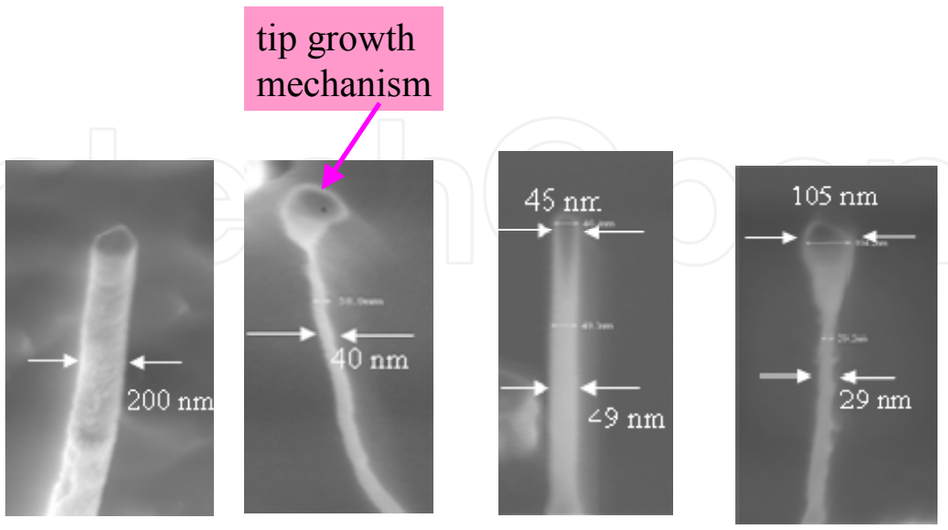

Fig. 6. Tube characteristics were engineered to some extent, via CNT growth parameters (pressure, catalyst thickness and power) and depict very wide ~ 200 nm tubes down to tubes only ~ 29 nm wide. A tip growth mechanism was also seen to be operative for Ni/Si (c. Kaul *et al.*, 2009).

4.2 Actuation in Vertical Carbon Nanofibers

By lithographically patterning the Ni catalyst sites, it is possible to produce a single, vertically aligned tube at a pre-defined location using DC PECVD, as described in Section 4.1. We now describe the electrostatic switching characteristics of such vertical NEMS structures which has the potential to increase integration density for 3D-electronics (a. Kaul *et al.*, 2009). Switching between vertically oriented tubes arranged in a 3-terminal configuration was recently reported (Jang *et al.*, 2005). In this work, a nanoprobe inside an SEM was mechanically manipulated in order to actuate a single, vertically oriented CNF. Nanomanipulation was also used to interrogate the electrical conduction in individual, as-grown CNFs grown on Si, as well as refractory nitride underlayers.

The tubes were synthesized with C_2H_2:NH_3 = 1:4 at 5 Torr and 700°C with Ni catalyst. Tubes were grown directly on Si <100> substrates with resistivity ρ ~ 1–5 m Ω-cm, and NbTiN. The ~ 200 nm thick refractory NbTiN was sputtered, with ρ ~ 113 μΩ-cm, and was also chemically compatible with CNF synthesis. The sample was mounted on a 45° beveled holder inside the SEM. A nanomanipulator probe stage (Kammrath and Weiss) was placed inside the scanning-electron-microscope (SEM) (FEI Quanta 200F), where tungsten probes were used to make *in situ* electrical measurements with an HP 4155C parameter analyzer.

The nanoprobe physically contacted an individual CNF grown on NbTiN, as shown by the SEM in the inset of Fig. 7 (ground probe was on substrate). Since the probe-to-tube contact length was < 100 nm for this 2-terminal measurement, conduction was dominated by the large contact resistance. The work function φ for tungsten (W) φ_W ~ 4.5 eV < φ_{CNF} ~ 5.0 eV (Ahmad *et al.*, 2007), and suggests a Schottky barrier may arise at this interface, and also

possibly at the tube-to-substrate interface; φ_{NbN} ~ 3.92 eV and like most transition metal nitrides with low φ (Saito *et al.*, 1999), it is likely $\varphi_{NbTiN} < \varphi_{CNF}$. A sub-gap region with suppressed conductance at low biases was seen in both polarities, and may have arisen from a native oxide on the W probes; if a small semiconducting junction (e.g. Schottky) also exists, an asymmetry in the I-V characteristic would arise, as observed.

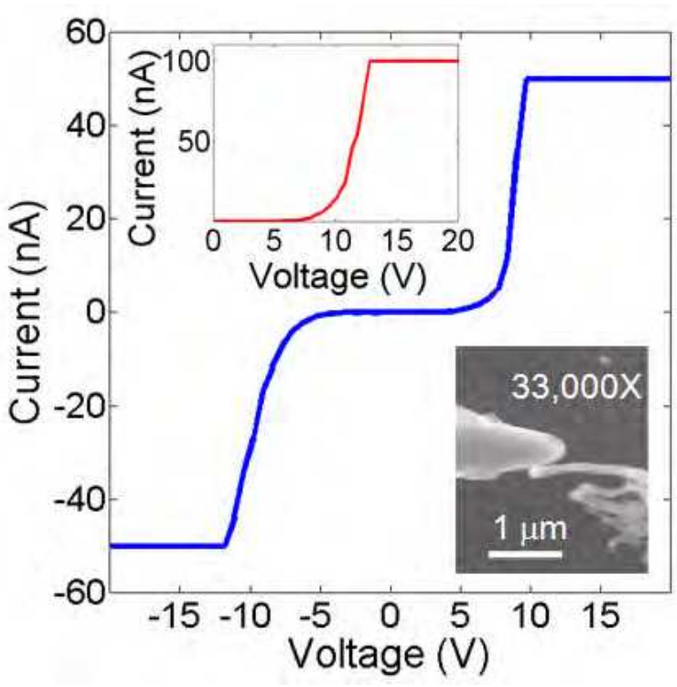

Fig. 7. Electrical continuity measurements for a single CNF grown on NbTiN. This tube is oriented vertically, so the image is rotated by 90°counter-clockwise. A nanoprobe is in contact with CNF, as indicated by the SEM image. The inset shows compliance increased to 100 nA.

Actuation measurements were performed for CNFs on NbTiN, where a nanoprobe was manipulated to within a few hundred nm of a single CNF. The electrostatic force per unit length F_{Elec} increases as $F_{Elec} \prec V^2$, where V is the voltage, and the elastostatic force per unit length F_{Elasto} increases as $F_{Elasto} \prec EI$, where E and I are the elastic modulus and moment of inertia of the nanotube, respectively (Dequesnes *et al.*, 2002). With increasing V ($F_{Elec} > F_{Elasto}$) the tube deflects closer to the probe, and a tunneling current is detected which increases exponentially, and results in a sudden or sharp change in slope at turn-on. The switching I-V in Fig. 8 shows currents rising sharply at V_{pi} ~ 18 V. The turn-off occurred at ~ 16 V and was dominated by the large tube-to-probe contact resistance since the tube remained stuck to the probe; thus, the turn-off response was similar to Fig. 7. The inset in Fig. 8 captures another switching event for a different tube, where turn-on and turn-off occurred at ~ 14 V and 10 V, respectively, and also illustrates the abruptness of the turn-on transition.

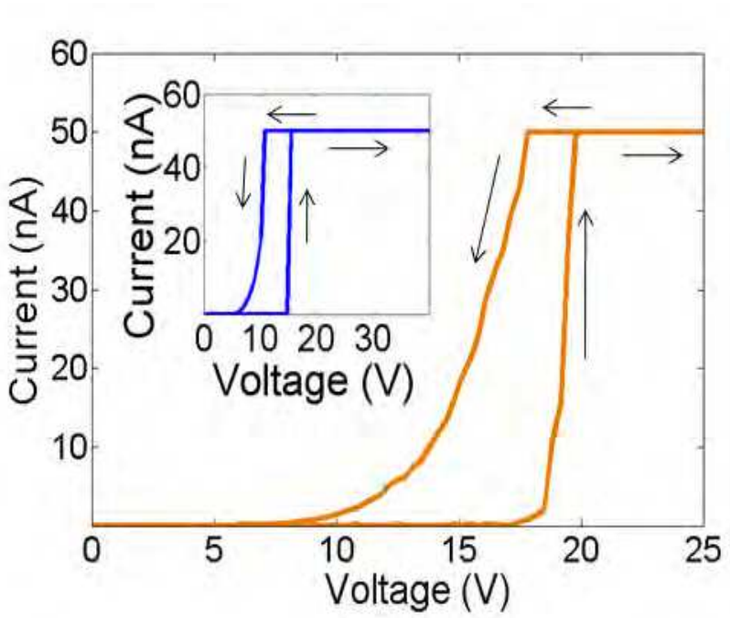

Fig. 8. Actuation test where a nanoprobe was within hundred's of nm of a CNF. Turn-on and turn-off were at ~ 18 V and 16 V, respectively, where turn-off was dominated by the tube-to-probe contact resistance. The inset shows another tube where turn-on and turn-off occurred at ~14 V and 10 V, respectively, and also indicates the abruptness of the turn-on transition (a. Kaul *et al.*, 2009).

The top SEM image in the inset of Fig. 9a shows a different tube with an initial gap g_0 ~ 220 nm between the probe and the tube, just before actuation, while the bottom SEM shows the tube stuck to the probe just after actuation. From the I-V, the switching voltage or onset of a current occurs at ~ 32 V (cycle 1). Although the bottom SEM image in the inset of Fig. 9a shows the tube stuck to the probe after actuation, with a contact length < 50 nm, it detached prior to the onset of the second actuation cycle (cycle 2). In cycle 2, V_{pi} ~ 35 V, but the turn-off was almost identical to cycle 1, since it was dominated by the contact resistance. When g_0 was increased to > 400 nm (SEM image in the inset of Fig. 9b), a switching event could not be detected, confirming the scaling trend of V_{pi} with g_0, to first order. From the I-V in Fig. 9b, we also deduce very low leakage currents in the instrumentation (< 150 pA peak-to-peak up to 40 V).

The SEM images depict stiction in the tubes after actuation, and suggests that the van der Waals force $F_{vdw} > F_{Elasto}$ which is validated by the hysteresis in the I-Vs of Fig. 7b and 8a. In earlier work (Jang *et al.*, 2005), stiction was also reported for vertically oriented tubes, but no hysteresis data was presented that electrically signaled the presence of stiction, as reported here. Nontheless, due to the apparently large magnitue of the van der Waals forces at these length scales, such structures appear to show promise for nonvolatile memory applications.

The nanomanipulation measurements conducted here also revealed that the tubes synthesized directly on Si were not electrically conducting as no currents could be detected up to 40 V when the probe touched a single tube. Thus, such measurements suggest that the

buffer layer of NbTiN resulted in tubes that were electrically conducting via the sidewalls and suitable for DC NEMS applicaitions for 3D electronics.

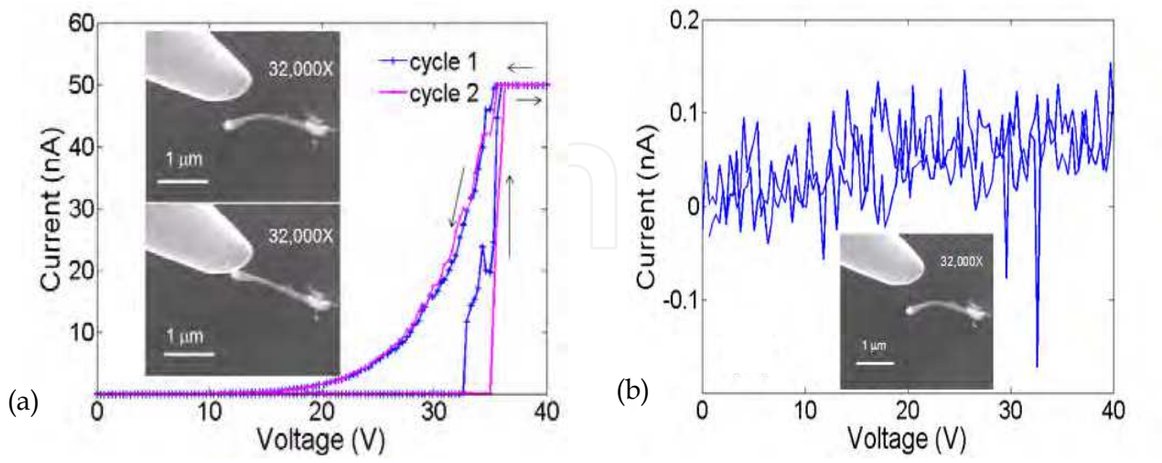

Fig. 9. a) The top SEM in the inset shows g_0 ~ 220 nm just before actuation. The bottom SEM in the inset shows the tube after actuation, where it was momentarily stuck to the probe, but detached prior to the onset of cycle 2. The I-V shows 2 switching cycles with turn-on varying slightly (~ 32 V and 35 V) but very little variation was seen in the turn-off cycles. b) The gap was increased further to > 400 nm, as shown by the SEM in the inset, where the I-V indicates the absence of switching and confirms the scaling of V_{pi} with g_0, to first order. From this, leakage currents in the instrumentation were < 150 pA (peak-to-peak) up to 40 V (a. Kaul *et al.*, 2009).

The nanomanipulation measurements conducted here also revealed that the tubes synthesized directly on Si were not electrically conducting as no currents could be detected up to 40 V when the probe touched a single tube. Thus, such measurements suggest that the buffer layer of NbTiN resulted in tubes that were electrically conducting via the sidewalls and suitable for DC NEMS applicaitions for 3D electronics.

5. Summary and Future Directions

This chapter provided an overview of the applications of suspended or free-standing CNTs as sensors and actuators. Firstly, a scheme for using 5-10 μm long, diffusively contacted SWNTs as thermal conductivity-based pressure sensors was presented. Pressure sensing was demonstrated over a wide dynamic range from atmosphere to 10^{-6} Torr by suspending the tubes. More work is necessary to fully characterize the effect of tube chirality, length and transparency at the contacts. However, in general, CNT based thermal vacuum gauges appear to be promising for pressure sensing, particularly for vacuum-encased microcavity applications. We also reviewed recent work on the use of laterally suspended tubes and NEMS beams for resonator applications, which have been applied to mass sensing, especially for biological applications.

Secondly, the actuator applications of suspended CNTs was also presented, namely those architectures where the tubes are oriented parallel to the substrate and those where they are

oriented vertically. The approaches used to suspend the tubes was discussed, including post-growth release. For SWNT air bridge NEMS switches, suspended tubes were grown across pre-fabricated trenches using patterned catalysts and materials that are compatible with the high temperature CVD synthesis of SWNTs. While these actuators were based on single, laterally suspended tubes, we also commented on the use of monolayer thick fabrics of tubes that are currently under development by companies such as Nantero for CMOS-CNT based mechanical memories.

Thirdly, we described the use of dc PECVD for forming isolated, vertically oriented tubes with manufacturable techniques, where such tubes have applications in 3D electronics. We experimentally demonstrated electrostatic switching in single, vertically oriented PECVD grown tubes on NbTiN substrates, where the hysteresis data presented suggests that such structures are promising for 3D nonvolatile memory applications. Nanomanipulation tests on individual tests also revealed tubes synthesized directly on Si by DC PECVD with ammonia and acetylene were electrically unsuitable for DC NEMS applications.

Challenges still lie ahead in our ability to control nanotube properties adequately (e.g. chirality, high contact resistance, and diameter) given the present day synthesis techniques. This will ultimately impact the large-scale integration of CNTs for end-use applications. While the prospect for nanotubes as promising components for future miniaturized electronic devices still remains high, recently attention has also focused on graphene, from which 1D CNTs are derived.

Graphene, like any monolayer-thick 2D-crystal was presumed to be thermodynamically unstable for many decades, but after the recent success in its synthesis, it has sparked tremendous excitement within the scientific community, given the exceptional electronic properties it posseses (Geim & Novoselov, 2007). In addition, the Young's modulus of suspended quasi-1D graphene nano-ribbons (GNR) was recently determined to be 7 TPa (Hod *et al.*, 2009), the highest known for any material. It is clear, just like the past several decades, carbon-based nanostructures will continue to be an area of intense scientific and technological interest for the foreseeable future.

Acknowledgements

We would like to thank the following people for the useful discussions and technical support they have provided during the course of the work that was presented in this chapter: Eric W. Wong, Abdur R. Khan, Krikor G. Megerian, Robert Kowalczyk, Leif C. Bagge, Henry G. LeDuc, Richard Baron, Ron Ruiz, Paul von Allmen, Julia R. Greer, Andrew T. Jennings, Guy De Rose, Bophan Chim, Michael J. Bronikowski, and Brian Hunt. The research described in this chapter was carried out at the Jet Propulsion Laboratory, California Institute of Technology, under a contract with the National Aeronautics and Space Administration.

6. References

Ahmed S., Das S., Mitra M. K., Chattopadhyay K. K. "Effect of temperature on the electron field emission from aligned carbon nanofibers and multiwalled carbon nanotubes." *Appl. Surf. Sci.*, 2007: 254, 610-615.

Alvesteffer W. J., Jacobs D. C., Baker D. H. "Miniaturized thin film thermal vacuum sensor." *J. Vac. Sci. Technol. A*, 1999: 13, 2980-2985.

Bachtold A., Hadley P., Nakanishi T., Dekker C. "Logic circuits with carbon nanotube transistors." *Science*, 2001: 294, 1317-20.

Cha S. N., Jang J. E., Choi Y., et al. "Fabrication of a nanoelectromechanical switch using a suspended carbon nanotube." *Appl. Phys. Lett.*, 2005: 86, 083105.

Collins P. G., Bradley K. B., Ishigamo M., Zettl A. "Extreme oxygen sensitivity of electronic properties of carbon nanotubes." *Science*, 2000: 287, 1801-1804.

Dequesnes M., Rotkin S. V., Aluru N. R. "Calculation of pull-in voltages for carbon-nanotube-based nanoelectromechanical switches." *Nanotech.*, 2002: 13, 120-131.

Dresselhaus M. S, Dresselhaus G., Avouris P. *Carbon Nanotubes.* Berlin: Springer, 2001.

Dujardin E., Derycke V. Goffman M. F., et al. "Self-assembled switches based on electroactuated multiwalled nanotubes." *Appl. Phys. Lett.*, 2005: 87, 193107.

Eriksson A., Lee S., S. Abdelrahim, *et al.* "Direct transmission detection of tunable mechanical resonance in an individual carbon nanofiber relay." *Nano Lett.*, 2008: 8, 1224-1228.

Esashi M., Sugiyama S., Ikeda K., Wang Y., Miyashita H. "Vacuum-sealed silicon micromachined pressure sensors." *Proc. IEEE*, 1998: 86, 1627-1639.

Geim A., Novoselov K. "The rise of graphene." *Nature materials*, 2007: 6, 183-191.

Grow R. J., Wang Q., Cao J., Wang D., Dai H. "Piezoresistance of carbon nanotubes on deformable thin-film membranes." *Appl. Phys. Lett.*, 2005: 86, 093104.

Hertel T., Walkup, R. E., Avouris, P. "Deformation of carbon nanotubes by survace van der Waals forces." *Phys. Rev. B*, 1998: 58, 13870-3.

Hierold C., Jungen A., Stampfer C., Helbling T. "Nano electromechanical sensors based on carbon nanotubes." *Sensors and Actuators A*, 2007: 136, 51-61.

Hod O., Scuseria G. "Electromechanical properties of suspended graphene nanoribbons." *Nano Lett.*, 2009: 9, 2619-2622.

Hofmann S., Ducati C., Robertson J., Kleinsorge B. "Low-temperature growth of carbon nanotubes by plasma-enhanced chemical vapor deposition." *Appl. Phys. Lett.*, 2003: 83, 135-137.

Homma Y., Chiashi S., Kobayashi Y. "Suspended single-wall carbon nanotubes: synthesis and optical properties." *Reports on Progress in Physics*, 2009: 72, 066502.

http://www.nantero.com/.

Ijima, S. "Helical microtubules of graphitic carbon." *Nature*, 1991: 354, 56-58.

Ilic B., Yang Y., Craighead H. G. "Virus detection using nanoelectromechanical devices." *Appl. Phys. Lett.*, 2004: 85, 2604-2606.

Jang J. E., Cha S. N., Choi Y. et al. "Nanoelectromechanical switches with vertically aligned carbon nanotubes." *Appl. Phys. Lett.*, 2005: 87, 163114.

a. Kaul A. B., Khan A., Bagge L., Megerian K., LeDuc H., Epp L. "Interrogating vertically oriented carbon nanofibers with nanomanipulation for nanoelectromechnical switching applications." *Appl. Phys. Lett.*, 2009: 95, 093103.

b. Kaul A. B., Manohara H. "Carbon nanotube vacuum gauges with wide dynamic range." *IEEE Trans. Nanotech.*, 2009: 8, 252-257.

c. Kaul A. B., Megerian K., Allmen P., Baron R. "Single, aligned carbon nanotubes in 3D nanoscale architectures enabled by top-down and bottom-up manufacturable processes." *Nanotech.*, 2009: 20, 075303.

d. Kaul, A. B. "Gas sensing with long, diffusively contacted single-walled carbon nanotubes." *Nanotech.*, 2009: 20, 155501.

Kaul A. B., Wong E., Epp L., Hunt B. "Electromechanical carbon nanotube switches for high-frequency applications." *Nano Lett.*, 2006: 6, 942-947.

Kawano T., Chiamori H. C., Suter M., *et al.* "An electrothermal carbon nanotube gas sensor." *Nano Lett.*, 2007: 7, 3686-3690.

Kawano T., Christensen D., Chen S., Cho C., Lin L. "Formation and characterization of silicon/carbon nanotube/silicon heterojunctions by local synthesis and assembly." *Appl. Phys. Lett.*, 2006: 89, 163510.

Kim P., Lieber C. M. "Nanotube nanotweezers ." *Science*, 1999: 286, 2148-2150.

Lee S. W., Lee D. S., Morjan R. E., Jhang S. H., Sveningsson M., Nerushev O. A., Park Y. W., Campbell E. E. B. "A three-terminal carbon nanorelay." *Nano Lett.*, 2004: 4, 2027-2030.

Lefebvre J., Homma Y., Finnie P. "Bright band gap photoluminescence from unprocessed single-walled carbon nanotubes." *Phys. Rev. Lett.*, 2003: 90, 217401-1-4.

Li J., Cassell A., Ng H. T., Stevens R., Han J., Meyyappan M. "Bottom-up approach for carbon nanotube interconnects." *Appl. Phys. Lett.*, 2003: 82, 2491-93.

Minot E. D., Yaish Y., Sazonova V., Park J. Y., Brink M., McEuen P. L. "Tuning carbon nanotube band gaps with strain." *Phys. Rev. Lett.*, 2003: 90, 156401.

Naik A., Hanay M., Hiebert W.,Feng X., Roukes M. "Towards single-molecule nanomechanical mass spectrometry." *Nature Nanotech.*, 2009: 4, 445-450.

Nygard J., Cobden D. H. "Quantum dots in suspended single-walled carbon nanotubes." *Appl. Phys. Lett.*, 2001: 79, 4216-8.

Odom T. W., Huang J. L., Kim P., Lieber C. M. "Atomic structure and electronic properties of single-walled carbon nanotubes." *Nature*, 1998: 391, 62-64.

Peng H. B., Chang C. W., Aloni S., Yuzvinsky T. D., Zettl A. "Ultrahigh frequency nanotube resonators." *Phys. Rev. Lett.*, 2006: 97, 087203.

Peroulis D., Pacheco S. P., Sarabandi K., Katehi L. P. B. "Electromechanical considerations in developing low-voltage RF MEMS switches." *IEEE Trans. on Microwave Theory and Tech.*, 2003: 51, 259-270.

Peterson, K. E. "Silicon as a mechanical material." *Proc. IEEE*, 1982: 70, 420-469.

Pop E., Mann D., Cao J., Wang Q., Goodson K., Dai H. J. "Negative differential conductance and hot phonons in suspended nanotube molecular wires." *Phys. Rev. Lett.*, 2005: 95, 155505.

Ren Z. F., Huang Z. P., Xu J. W., Wang J. H., Bush P., Siegal M. P., Provencio P. N. "Synthesis of large arrays of well-aligned carbon nanotubes on glass." *Science*, 1998: 282, 1105-1107.

Rueckes T., Kim K., Joselevich E., Tseng G.Y., Cheung C. L., Lieber C. M. "Carbon nanotube-based nonvolatile random access memory for molecular computing." *Science*, 2000: 289, 94-97.

Saito Y., Kawata S., Nakane H., Adachi H. "Emission characteristics of niobium nitride field emitters." *appl. Surf. Sci.*, 1999: 146, 177-181.

Salvetat J.P., Bonard J. M., Thomson N. H., Kulik A. J., Forro L., Benoit W., Zuppiroli L. "Mechanical properties of carbon nanotubes." *Appl. Phys. A.*, 1999: 69, 255-260.

Sazonova V., Yaish Y., Ustunel H., Roundy D., Arias T. A., McEuen P. L. "A tunable carbon nanotube electromechanical oscillator." *Nature*, 2004: 431, 284-287.

Stampfer C., Helbling T., Obergfell D., *et al.* "Fabrication of single-walled carbon nanotube based pressure sensors." *Nano Lett.*, 2006: 6, 233-237.

Tombler T. W., Zhou C. W., Alexseyev L., Kong J., Dai H. J., Lei L., Jayanthi C. S., Tang M. J., Wu S. Y. "Reversible electromechanical characteristics of carbon nanotubes under local-probe manipulation." *Nature*, 2000: 405, 769-772.

Walters D. A., Ericson L. M. , Casavant M. J., Liu J., Colbert D. T., Smith K. A., Smalley R.E. "Elastic strain of freely suspended single-wall carbon nanotube ropes." *Appl. Phys. Lett.*, 1999: 74, 3803-3805.

Yu M. F., Lourie O., Dyer M. J., Moloni K., Kelly T. F., Ruoff R. S. "Strength and breaking mechanism of multiwalled carbon nanotubes under tensile load." *Science*, 2000: 287, 637-640.

Yu, C. Saha, S. Zhou, J., Shi, L., Cassel, A., Cruden, B. A. *et al.* "Thermal contact resistance and thermal conductivity of a carbon nanofiber." *J. Heat Transfer*, 2006: 128, 234-239.

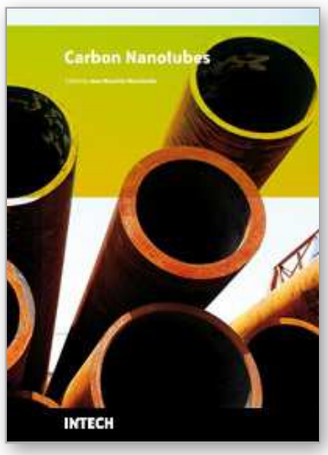

Carbon Nanotubes

Edited by Jose Mauricio Marulanda

ISBN 978-953-307-054-4
Hard cover, 766 pages
Publisher InTech
Published online 01, March, 2010
Published in print edition March, 2010

This book has been outlined as follows: A review on the literature and increasing research interests in the field of carbon nanotubes. Fabrication techniques followed by an analysis on the physical properties of carbon nanotubes. The device physics of implemented carbon nanotubes applications along with proposed models in an effort to describe their behavior in circuits and interconnects. And ultimately, the book pursues a significant amount of work in applications of carbon nanotubes in sensors, nanoparticles and nanostructures, and biotechnology. Readers of this book should have a strong background on physical electronics and semiconductor device physics. Philanthropists and readers with strong background in quantum transport physics and semiconductors materials could definitely benefit from the results presented in the chapters of this book. Especially, those with research interests in the areas of nanoparticles and nanotechnology.

INTECH
open science | open minds

InTech Europe
University Campus STeP Ri
Slavka Krautzeka 83/A
51000 Rijeka, Croatia
Phone: +385 (51) 770 447
Fax: +385 (51) 686 166
www.intechopen.com

InTech China
Unit 405, Office Block, Hotel Equatorial Shanghai
No.65, Yan An Road (West), Shanghai, 200040, China
中国上海市延安西路65号上海国际贵都大饭店办公楼405单元
Phone: +86-21-62489820
Fax: +86-21-62489821

IntechOpen